Article

Research on the Combustion Performance of Municipal Solid Waste in Different Sorting Scenarios: Thermokinetics Investigation via TG−DSC−FTIR−MS

Bingshuo Li, Wenkuo Zhang, Fan Jia, Tianhua Yang,* Suping Bai, and Quan Zhou

Read Online

ACCESS | Metrics & More | Article Recommendations

ABSTRACT: Waste sorting is regarded as one of the most important strategies for municipal solid waste (MSW) management. The changes in the combustion parameters after MSW sorting had a significant impact on the actual operation of the boiler. In the present study, the effects of heating rate on combustion characteristics and dynamics of MSW in different sorting scenarios were studied using the thermogravimetry (TG)−differential scanning calorimetry (DSC)−Fourier transform infrared (FTIR)−mass spectrometry (MS) technique. TG−DSC analysis showed that the heat released from MSW combustion at different heating rates ranged from 1394.1 to 4130.1 J/g. According to the TG−DTG curves, the combustibility of 30% sorted MSW was increased by 1.2 times compared to that of the unsorted scenario. In the 30% sorted scenario, the average activation energies were estimated to be 161.24 and 159.93 kJ/mol based on the Flynn−Wall−Ozawa (FWO) and Kissinger−Akahira−Sunose (KAS) methods, respectively. Based on the Coats−Redfern (CR) method, the minimum activation energies for unsorted and 20% sorted scenarios were 148.74 and 135.53 kJ/mol at 523 to 606 K, respectively, while they were 29.42 and 33.22 kJ/mol at 606 to 780 K. XRF analysis showed that the alkali and alkaline earth metal oxides in the ash contributed to a high risk of slagging and scaling. This work can provide a scientific basis for the real situation of MSW incineration.
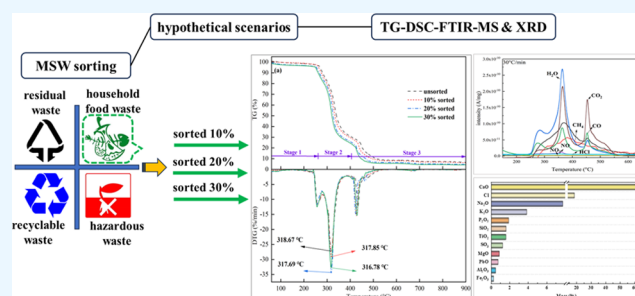
1. INTRODUCTION

Globally, municipal solid waste (MSW) generation is expected to increase to 9.5 billion tons per year by 2050,[1] with China accounting for more than a quarter of global MSW production. In the last decades, the volume removal and harmless treatment of MSW in China maintained an upward trend from 2010 to 2019. The volume of MSW removal had increased from 158 million tons in 2010 to 242 million tons in 2019, which was relevant to the growing population and urbanization. At the same time, the rate of harmless disposal of MSW also increased from 77.9% in 2010 to 99.7% in 2020. In response to the year-on-year increase of MSW, in 2017, the National Development and Reform Commission and the Ministry of Housing and Urban-Rural Development jointly issued the "Implementation Plan of Domestic Waste Sorting System", which formulated a plan for the implementation of MSW sorting. In addition, Shanghai passed the *Regulations of Shanghai Municipality on the Management of Domestic Waste* in 2019. By 2022, most of China's 46 key cities had promoted and completed local special legislation on MSW sorting. By the end of 2025, cities at the prefecture level and above in China will basically establish an MSW sorting and treatment system.

According to the sorting process of Shanghai in China, MSW is mainly divided into four types: household food waste, residual waste, recyclable waste, and hazardous waste.[2] The moisture content of MSW after sorting was significantly reduced, and the calorific value of MSW was also significantly increased. The increase in the calorific value can improve the power generation per ton of MSW and the profitability of MSW-to-energy plants. With the separation of household food waste, the original concentration of particulate matter and acid gas will be decreased, which is beneficial to improving the boiler heat exchange efficiency and prolonging the boiler life, thus ensuring the long-term stable operation of the whole system.

Many scholars have focused on studying the combustion characteristics of MSW and using typical components of MSW to simulate actual MSW. The combustion performance of

Table 1. Proximate and Ultimate Analysis of Components of MSW

material	proximate analysis (wt %, d)				ultimate analysis (wt %, d)						HHV (MJ/kg)[c]
	M	A	V	FC[a]	C	H	O[b]	N	S	Cl	
paper	3.63	11.02	84.52	0.83	35.53	4.83	44.99	n.a.	n.a.	n.a.	12.77
cloth	3.38	2.79	84.62	9.21	39.55	5.65	48.39	0.24	n.a.	n.a.	14.76
chopstick	5.06	1.46	79.46	14.02	47.49	5.93	40.04	0.03	n.a.	n.a.	18.60
PE	n.a.	n.a.	100	n.a.	85.70	14.30	n.a.	n.a.	n.a.	n.a.	46.79
PVC	n.a.	n.a.	94.9	5.1	39.60	4.90	n.a.	0.5	1.8	53.2	19.86
residual waste	2.23	2.58	89.5	5.69	54.06	8.47	34.59	0.24	n.a.	n.a.	25.05
household food waste	2.17	6.32	82.32	9.19	48.94	7.30	34.04	3.20	n.a.	n.a.	22.19

[a]FC = 100% − A − M − V. [b]O = 100% − M − A − S − N − C − H. [c]HHV = 35.2C + 116.2H + 6.3N + 10.5S − 11.1O;[16] d, dry basis; n.a., not available.

MSW can be evaluated by four combustion performance indicators: combustibility, comprehensive combustion index, ignition index, and burnout index.[3] Thermogravimetry analysis (TGA) was used to study the combustion process of MSW, which was helpful to analyze the combustion mechanism and obtain the kinetic parameters.[4,5] The components of MSW and the heating rate were the main factors affecting the combustion process and product properties of MSW.[6] The main thermal reaction temperature of MSW components was concentrated in the range of 150−500 °C, but the thermal stability properties of different components were quite different.[6−8] According to TG analysis of typical components, it was found that food residue presented multiple peaks below 320 °C, printing paper presented the main peak at 350 °C, and polyethylene (PE) and polypropylene (PP) presented a very strong peak at 455 to 485 °C.[9] In addition, the ignition difficulty of MSW components was ranked in the order of kitchen waste < wood, bamboo < paper < fabric < plastic. It was found that a single thermal measurement technique could obtain less information about material combustion properties. Boumanchar et al.[10] adopted the thermogravimetry−differential scanning calorimetry (TG−DSC) method to investigate the kinetic and thermal behavior of different kinds of MSW. TG−DSC analyses could use different types of fuels at different heating ratios under an oxidative atmosphere to gather thermal and mass loss data.[11] Thermogravimetric analysis coupled with Fourier transform infrared (TG−FTIR) spectroscopy was also used to identify the real-time gaseous products during the co-combustion of MSW and hydrochar.[7] Cheng et al.[12] studied the combustion characteristics of the oil sludges and semicokes during ignition and subsequent burning in detail by using thermogravimetry−differential scanning calorimetry−mass spectrometry (TG−DSC−MS) technology and quantitatively determined a series of combustion characteristic parameters and the derived comprehensive indexes. Combining the single TGA with FTIR, MS, and other technologies can continuously measure the mass and heat changes of substances while detecting the composition of the gaseous products online in real time.[13−15]

Previous studies mostly focused on the combustion characteristics and dynamic analysis of primary MSW, while there were few reports on the combustion characteristics and multicomponent dynamic analysis of sorted MSW. In recent years, China has been accelerating the implementation of MSW sorting, and it is of great significance to investigate the combustion performance of sorted MSW. In the present study, TG−DSC−FTIR−MS technology was used to study the combustion characteristics of MSW, and to discuss the influence of heating rate and assumed different sorting

scenarios on the combustion process. The reaction activation energy was calculated using the model Coats−Redfern (CR) method and two model-free methods of Flynn−Wall−Ozawa (FWO) and Kissinger−Akahira−Sunose (KAS).

2. MATERIAL AND METHODS

2.1. Materials. Several typical wastes (paper towels, wooden chopsticks, cotton cloth, PE, poly(vinyl chloride) (PVC), leftovers, and vegetable peels) were collected from Shenyang, China, which were used as components of the MSW in the experiment. The raw material was dried, ground into small particles, and sieved to less than 100 meshes (75 μm). According to the real compositions of MSW in Tianjin City, the ratio of household food waste to residual waste was 1:1. The proportion of residual waste (the share of nonincinerable waste was removed) in MSW was determined as paper towels/wood chopsticks/waste plastics/cotton cloth = 0.41:0.04:0.45:0.1. Leftovers, vegetable leaves, and peels were mixed as household food waste. The combustion performance of MSW in three scenarios according to the wet garbage sorting ratio (0, 10, 20, and 30%) was considered according to the current sorting situation in China. The characteristics of components of MSW are shown in Table 1.

2.2. Experimental Methods. A combination of TG−DSC−FTIR−MS (STA449F TG−DTG, iS50FTIR infrared analyzer, and QMS-403D-Aeolos) was used to carry out combustion experiments of MSW under different conditions. The samples (10 ± 0.01 mg) were placed into an Al_2O_3 crucible and heated in an argon and oxygen mixed atmosphere from 40 to 900 °C at a heating rate of 10, 20, and 30 °C/min, respectively. The infrared spectrum resolution was 8 cm^{-1}, and the wavelength range was 4000−400 cm^{-1}. The mass spectrometer was operated at a 70 eV electron energy.

The compositions of ash generated from the combustion of MSW samples under different conditions were measured with an X-ray fluorescence spectrometer (XRF, Japanese Rigaku ZSX Primus IV).

2.3. Combustion Performance Index. The following four combustion performance indicators were adopted: combustibility (C), comprehensive combustion index (CCI), ignition index (D_i), and burnout index (D_b), as shown in eqs 1−4.[3]

$$C = -R_p/T_i^2 \tag{1}$$

$$CCI = -R_p \times (R_v)/(T_i^2 \times T_p) \tag{2}$$

$$D_i = -R_p/(t_i \times t_p) \tag{3}$$

Table 2. Common Reaction Models

| symbol	mechanism	$f(\alpha)$	$G(\alpha)$
		diffusion model	
D1	one-dimensional diffusion	$1/(2\alpha)$	α^2
D2	two-dimensional diffusion	$[-\ln(1-\alpha)]^{-1}$	$(1-\alpha)\ln(1-\alpha)+\alpha$
D3	three-dimensional diffusion	$[(3/2)(1-\alpha)^{2/3}][1-(1-\alpha)^{1/3}]$	$[1-(1-\alpha)^{1/3}]^2$
D4	Ginstling−Brounstein	$[(3/2)(1-\alpha)^{1/3}][1-(1-\alpha)^{1/3}]$	$(1-2\alpha/3)-(1-\alpha)^{2/3}$
		geometrical contraction model	
R2	contracting cylinder	$2(1-\alpha)^{1/2}$	$1-(1-\alpha)^{1/2}$
R3	contracting sphere	$3(1-\alpha)^{1/3}$	$1-(1-\alpha)^{1/3}$
		reaction order model	
F1	first-order reaction	$1-\alpha$	$-\ln(1-\alpha)$
F2	second-order reaction	$(1-\alpha)^2$	$(1-\alpha)^{-1}-1$
F3	third-order reaction	$(1-\alpha)^3$	$[(1-\alpha)^{-2}-1]/2$
Fn	nth-order reaction	$(1-\alpha)^n$	$[1-(1-\alpha)^{1-n}-1]/(1-n)$
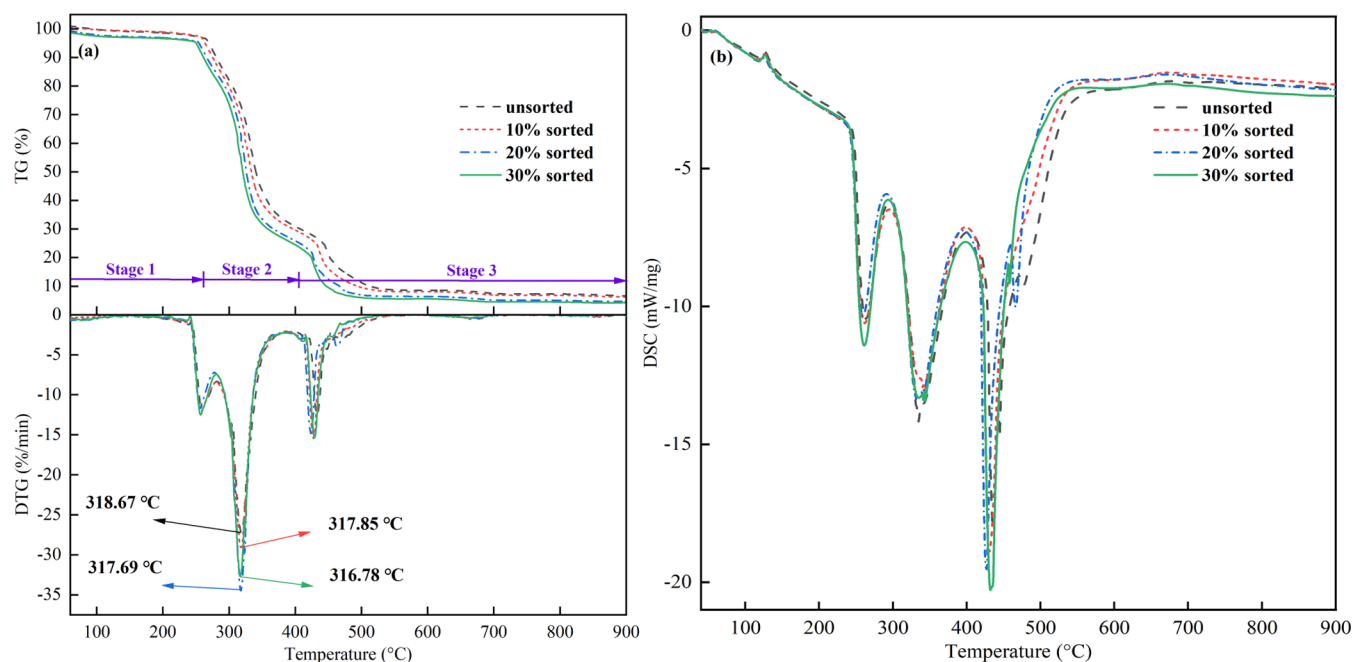
Figure 1. (a) TG−DTG and (b) DSC curves of MSW in different sorting scenarios.

$$D_b = -R_p/(\Delta t_{1/2} \times t_p \times t_b) \tag{4}$$

where R_p and R_v are the maximum and average weight loss rates, respectively; T_i and T_b are the ignition temperature and burnout temperature, respectively; t_i is the ignition time; t_b is the burnout temperature; t_p is the maximum peak time for the reaction to proceed at the maximum rate; and $\Delta t_{1/2}$ is the half-peak width time range 1/2 (when the weight loss rate reaches 1/2 of the maximum weight loss rate).

2.4. Kinetics Analysis. In this study, two model-free fitting methods were used: FWO model and KAS model.[17−19]

$$\text{FWO: } \log \beta = \log(AE_a/R_g(\alpha)) - 2.315$$
$$- 0.4567E_a/(RT) \tag{5}$$

$$\text{KAS: } \ln(\beta/T^2) = \ln(AE_a/R_g(\alpha)) - E_a/(RT) \tag{6}$$

The CR method was used to determine the reaction mechanism. Assuming $2RT/E_a = 0$, the CR method can be described as follows:

$$\ln(g(\alpha)/T^2) = \ln(AR/E_\beta) - E/(RT) \tag{7}$$

where E was estimated based on the slope of the best fit line of the $\ln(g(a)/T^2)$ and $1/T$ curve. Table 2 shows the common reaction mechanism models in the solid-state process.[20] In this study, the model R2 was chosen to describe the reaction mechanism of the thermal degradation of the sample.[20]

3. RESULTS AND DISCUSSION

3.1. Combustion Characteristics. *3.1.1. Combustion Characteristics of MSW in Different Sorting Scenarios.* The TG−DTG−DSC curves of the combustion of MSW in different sorting scenarios in air at 20 °C/min are shown in Figure 1. The trend of the TG curves remained almost unchanged with the increased sorting ratio of household food waste from 0 to 30%. The combustions were divided into the following four stages: the first stage of water evaporation at 40−240 °C, the second stage of degradation and combustion of volatile matter at 240−324 °C, the third stage of the formation and combustion of chars at 324−500 °C, and the fourth stage of the degradation of inorganic components and

residual carbon above 500 °C.[21] The rapid decline of the second TG curve and the corresponding peak of DTG were mainly due to the cracking of alkanes, olefins, and other flammable small molecular compounds from the polymer.[22] Though household food waste was sorted out by the ratio of 0, 10, 20, and 30%, the corresponding temperature of the DTG maximum weight loss rate was 317.85, 317.69, and 316.78 °C, respectively, which were similar compared to the unsorted temperature of 318.67 °C.

There were three concentrated exothermic peaks in the DSC curves of MSW, among which the first and second represented the exothermic combustion of volatiles, and the third represented the combustion of fixed carbon. The exothermic area of the first and second exothermic peaks was larger than that of the third exothermic peak, which was related to the higher content of volatiles in MSW, indicating that the exothermic heat release in the combustion stage of volatiles in MSW was significant. It could be seen from the DSC curves that the MSW combustion had been in an exothermic process, and the reaction temperature corresponding to the maximum weight loss peak and the exothermic peak differed by 5−13 °C, which was due to the difference in the exothermic mechanism of small molecular organic compounds and macromolecular organic compounds. With the change in sorting ratio, the change in endothermic heat was small, and the endothermic heat was about 2600 J/g.

Table 3 lists the combustion characteristic parameters of MSW in different sorting scenarios. After sorting, the ignition

Table 3. Combustion Characteristic Parameters of MSW in Different Sorting Scenarios

indicators	sorting scenarios			
	0%	10%	20%	30%
C (10^{-4} %/(min °C^2))	3.71	3.88	4.06	4.43
CCI (10^{-6} %/(min^2 °C^3))	1.73	1.83	1.99	2.16
D_i (10^{-1} % min^{-3})	1.70	1.79	1.99	2.05
D_b (10^{-2} % min^{-4})	5.74	7.04	9.94	8.99
$-R_p$ (%/min)	27.24	29.08	34.47	32.66
$-R_v$ (%/min)	2.37	2.37	2.37	2.37
temperature (°C)				
T_i	271.01	273.88	291.28	271.46
T_b	507.27	501.05	483.09	485.38
T_p	318.67	317.85	317.69	316.78
time (min)				
t_i	11.59	11.75	12.55	11.61
t_b	23.51	23.19	22.26	22.40
t_p	13.83	13.81	13.79	13.75
$\Delta t_{1/2}$	1.46	1.29	1.13	1.18

temperature of MSW was increased. C, CCI, D_i, and D_b are the largest in the sorting scenario of 30%, which were 4.43×10^{-4} %/(min °C^2), 2.16×10^{-6} %/(min^2 °C^3), 2.05×10^{-1} % min^{-3}, and 8.99×10^{-2} % min^{-4}, respectively. This was because the volatile content of the MSW was increased after MSW sorting. The evaporation rate of volatiles was accelerated in the combustion process, and the heat generated by volatile combustion would accelerate the combustion of fixed carbon components. The C value of MSW was increased by 1.2 times when the sorting ratio was increased to 30%. However, the ignition temperature of MSW after sorting showed a trend of increasing and then decreasing. This was because the volatile content of MSW after sorting was increased and the energy

required for volatilizing was higher; therefore, the ignition temperature was increased from 271.01 to 291.28 °C. After MSW sorting, the combustion performance parameters were improved, which was beneficial to the combustion process.

3.1.2. Combustion Characteristics at Different Heating Rates. Figure 2 shows the TG−DTG−DSC curves of 30% sorted MSW at different heating rates (10, 20, and 30 °C/min). The heating rate had a significant effect on the combustion performance of MSW. As the heating rate increased, the DTG peak moved to higher temperatures. When the heating rate was 10, 20, and 30 °C/min, the peak temperatures corresponding to the maximum weight loss rate were 324.20, 334.20, and 341.40 °C, respectively. The peak temperature of the sample increased with the increase of the heating rate, which was common in nonisothermal heating, mainly due to the thermal lag phenomenon.[8,23] At a low heating rate, the temperature gradient between the particles was small, and the temperature difference between the inside and the outside of the particles was small,[24] forming a good heat transfer from the surface to the inside. On the contrary, at a high heating rate, a relatively higher temperature gradient made the temperature difference between the inside and outside of the particles larger, resulting in a lag in the reaction.[25]

The DSC curve of 30% sorted MSW at 20 °C/min showed that the peak temperatures of volatile matter release and char combustion were 355.9 and 438.3 °C, respectively, which were higher than the DTG peak temperatures of 339.3 and 435.3 °C, respectively. This was because the hysteresis effect between the external and internal particles hindered the release of heat. The heat release of the first, second, and third peaks of MSW accounted for 42.5, 13.1, and 44.4% of the total heat release, respectively. As the heating rate increased, the total heat released by the combustion of MSW ranged from 1394.1 to 4130.1 J/g because the combustion reaction became more intense with the increase of the heating rate.

3.2. Kinetics Analysis. *3.2.1. Kinetic Analysis at Different Heating Rates.* Figure 3 shows the reaction kinetic curves of different kinetic equations, with a conversion ratio of 0.1−0.6. The FWO and KAS conversion rate methods were used to calculate the activation energy and pre-exponential factors at different heating rates (Table 4). The calculation of activation energy (E) (energy barrier of a chemical reaction) and pre-exponential factor (A) (collision frequency between activated molecules) can provide a reference value for actual optimization and design problems. The R^2 values of estimated values E and A were both greater than 0.9 by the methods of FWO and KAS. The estimated values obtained by using two equal conversion rate methods for MSW were 113.8−194.88 kJ/mol, respectively. The average value of 30% sorted MSW reached its minimum and maximum values at conversion ratios of 0.2 and 0.6, respectively.

3.2.2. Dynamic Analysis in Different Sorting Scenarios. The combustion kinetic curves under different sorting scenarios are shown in Figure 4. The best fit correlation coefficients and the corresponding reaction series n, E, and A of the combustion reaction kinetics of MSW in different sorting scenarios are shown in Table 5. The correlation coefficients of the fitting equations were all above 0.95, indicating that the fitted effect was better. The components in the MSW were controlled by different reactions, which can be described by two to three first-order reactions, which were the same as the previous research results.[6,26]
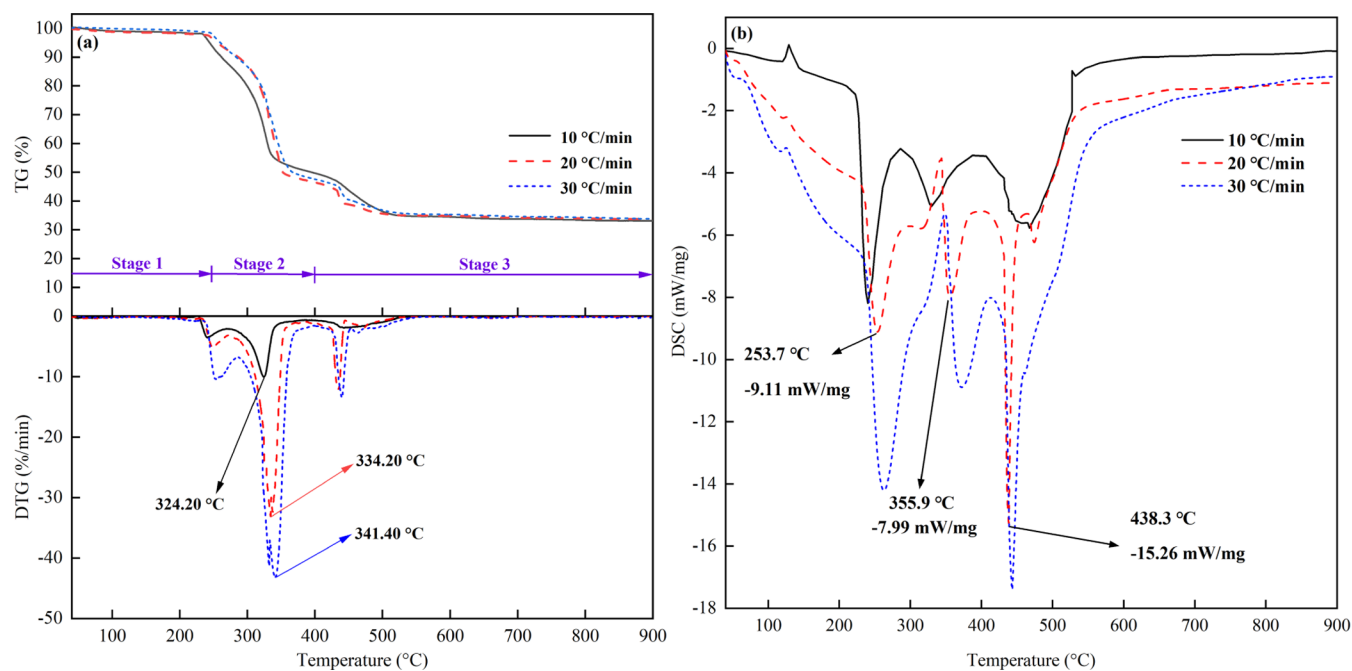
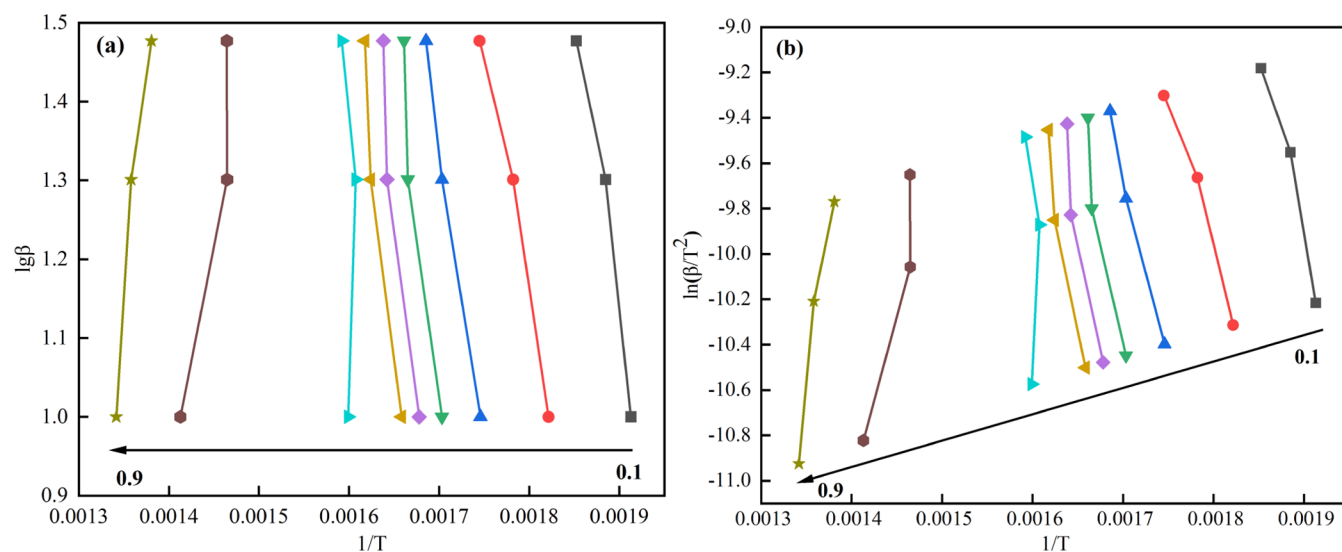**Figure 2.** (a) TG, DTG, and (b) DSC curves at different heating rates (30% sorted).

Figure 3. Combustion kinetic curves of different kinetic equations in a 30% sorted scenario: (a) FWO and (b) KAS.

Table 4. Combustion Kinetics of 30% Sorted MSW at Different Heating Rates

sample	α	FWO			KAS		
		E (kJ/mol)	A/s^{-1}	R^2	E (kJ/mol)	A/s^{-1}	R^2
30% sorted	0.1	142.40	1.24×10^{16}	0.963	141.04	1.24×10^{17}	0.958
	0.2	113.80	8.46×10^{12}	0.983	110.40	1.37×10^{9}	0.979
	0.3	141.28	1.37×10^{15}	0.993	138.85	1.17×10^{14}	0.991
	0.4	182.11	5.16×10^{18}	0.922	181.57	1.26×10^{22}	0.914
	0.5	192.99	3.72×10^{19}	0.923	192.99	8.42×10^{23}	0.916
	0.6	194.88	4.44×10^{19}	0.951	194.72	8.17×10^{23}	0.946
	average	161.24	1.45×10^{19}		159.93	2.79×10^{23}	

3.3. MSW Combustion Products Analysis. *3.3.1. FTIR Analysis.* The gaseous product of 30% sorted MSW at a heating rate of 20 °C/min is shown in Figure 5. In the volatile combustion stage, the weight loss rate of MSW was the highest and the combustion reaction was the fastest. Moreover, the analysis of the main functional groups of MSW at different temperatures showed that the peak value of each product was the largest when the temperature was 330 °C; therefore, the functional groups of products changed obviously at 330 °C. The infrared peak of CO_2 was much higher than the peaks of
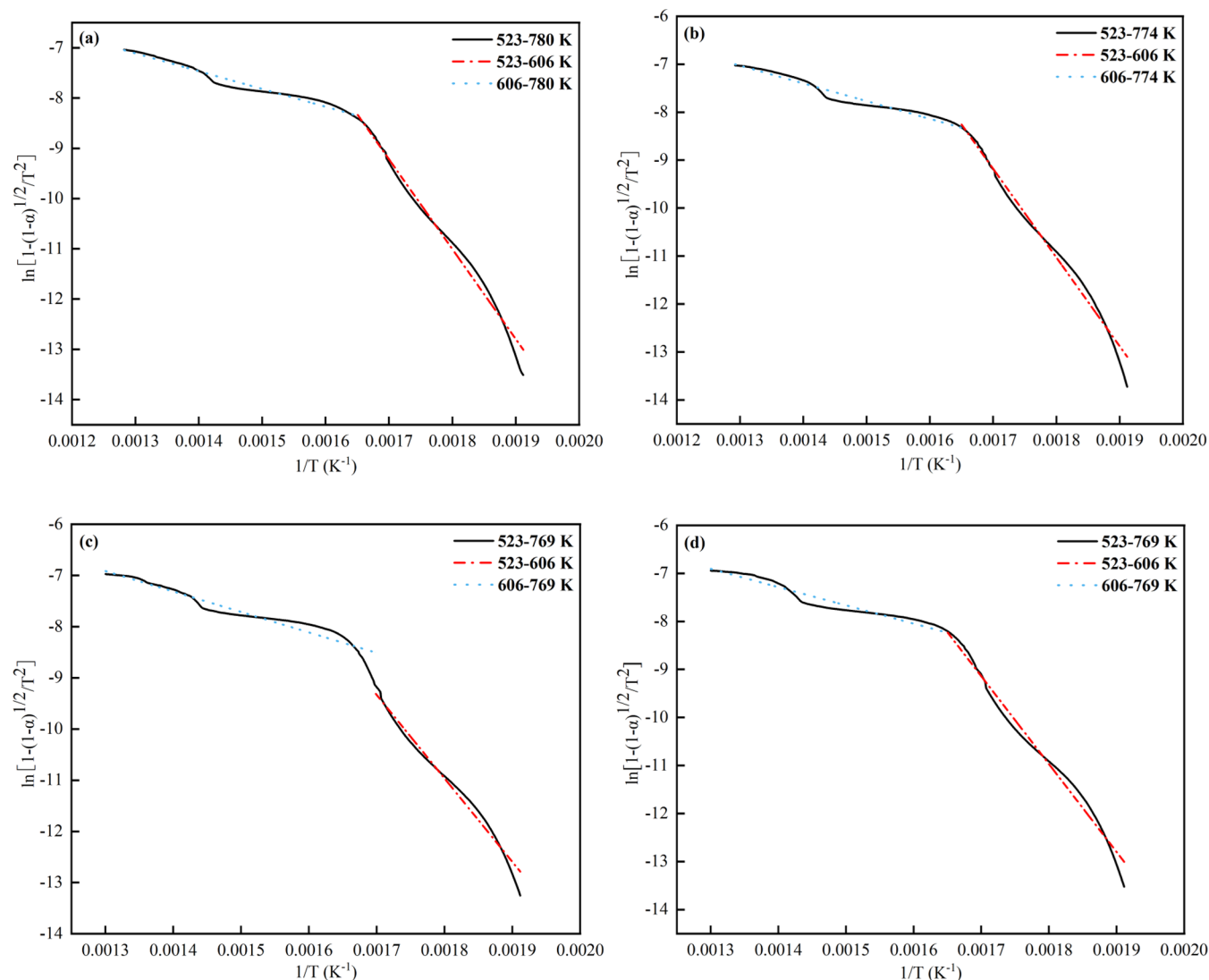
Figure 4. Combustion kinetic curves in different sorting scenarios: (a) unsorted, (b) 10% sorted, (c) 20% sorted, and (d) 30% sorted.

Table 5. Kinetic Parameters of MSW Combustion in Different Sorting Scenarios

sample	temperature (K)	fit equation	E (kJ/mol)	A/min^{-1}	R^2
unsorted	523−606	$Y = 21.19 - 17\,890.3X$	148.74	2.85×10^{11}	0.987
	606−780	$Y = -2.51 - 3538.82X$	29.42	2.88	0.965
10% sorted	523−606	$Y = 22.25 - 18\,492.34X$	153.74	8.51×10^{11}	0.987
	606−774	$Y = -2.22 - 3700.3X$	30.76	4.02	0.957
20% sorted	523−606	$Y = 18.38 - 16\,301.96X$	135.53	1.57×10^{10}	0.983
	606−769	$Y = -1.72 - 3995.85X$	33.22	7.16	0.934
30% sorted	523−606	$Y = 21.93 - 18\,278.18X$	151.96	6.11×10^{11}	0.986
	606−769	$Y = -1.97 - 3800.12X$	31.59	5.3	0.941

other functional groups, indicating that the main product in the combustion process was CO_2. The generation of some alkanes and aromatic compounds was due to the release of volatiles at a lower temperature.

The main functional groups of combustion products at different heating rates were similar; herein, the main functional groups detected and their related gases obtained at a heating rate of 20 °C/min were analyzed, as shown in Table 6. The absorption band ranged from 4000 to 3400 cm^{-1} corresponding to O−H tensile vibration, indicating the formation of H_2O. C−H tensile vibrations were detected in the range of 3150−

2700 cm^{-1}, which showed the appearance of CH_4. The formation of CH_4 was mainly attributed to the cleavage of stable methylene and weak methoxy groups. The ranges of 2400−2220 cm^{-1} and 780−600 cm^{-1} belonged to the C−O tensile vibration of CO_2, which was due to the breaking or reforming of C=O and C−O−C.[20] The C−O tensile vibration of 2220−2000 cm^{-1} indicated CO emissions. Incomplete combustion of fixed carbon and C_xH_y were the main causes of CO emissions.[27] The ranges of 1900−1600 cm^{-1} and 1600−1480 cm^{-1} were related to the stretching vibration of C=O and C−C benzene skeletons, respectively,
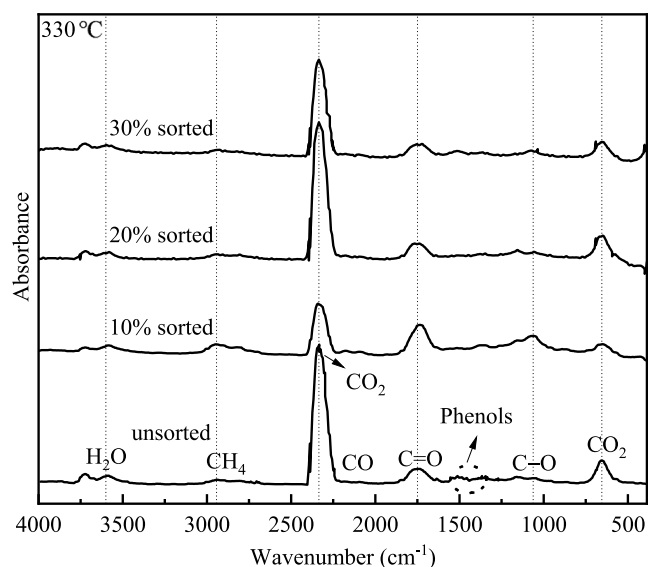
**Figure 5.** FTIR spectrum of gaseous products at 330 °C of 30% sorted MSW.

Table 6. FTIR Spectroscopy Analysis of Main Functional Groups

wavenumber (cm^{-1})	functional group	product	maximum peak (cm^{-1})
4000–3400	O–H stretching vibration	H_2O	3730
3150–2700	C–H asymmetric stretching vibration	CH_4	2910
2400–2220	C═O stretching vibration	CO_2	2310
2220–2000	C–O stretching vibration	CO	2116
1900–1600	C═O stretching vibration	aldehydes, ketones, acids	1768
1600–1480	C–C benzene skeleton stretching vibration	aromatics	1530
1480–1000	C–C, C–O benzene skeleton stretching vibration	alkanes, alcohols, phenols, ethers, lipids	1163
780–600	C═O asymmetric stretching vibration	CO_2	637

indicating the formation of carbonyl-containing compounds (aldehydes, ketones, and acids) and aromatic hydrocarbons. The C–O, C–C, and C–chain skeletal bending vibrations detected in the range of 1480–1000 cm^{-1} corresponded to the presence of alkanes, alcohols, ethers, phenols, and lipids.[28]

3.3.2. Mass Analysis. The release of gaseous products from the combustion of 30% sorted MSW samples at different heating rates was simultaneously monitored by TG–MS. From Figure 6, the gaseous products were mainly released in the temperature range of 150–600 °C. It can be considered that the gaseous products were mainly composed of light volatile compounds as H_2O ((m/z) = 18), hydrocarbons as CH_4 ((m/z) = 16), acidic compounds as HCl ((m/z) = 37), carbon oxides as CO and CO_2 ((m/z) = 28 and 44), and nitrogen-containing compounds as NO and NO_2 ((m/z) = 30 and 46). The gas products obtained at different heating rates were also similar. By analyzing the mass spectrum of the 30% sorted MSW at a heating rate of 20 °C/min, it can be observed that H_2O and CO_2 were the most emitted gaseous products. The mass-to-charge ratio peak of 18 was consistent with the DTG curve. The first peak at 200–250 °C mainly corresponded to the precipitation of external and internal water in MSW, and the second peak at 250–550 °C was mainly due to the conversion of oxygen-containing functional groups. With the heating rate increasing to 30 °C/min, the temperature corresponding to the peak moved to the higher-temperature region, and the peak temperature of the main gaseous products increased from 350 to 370 °C, which was also similar to the TG analysis.

3.4. Ash Composition Analysis. As shown in Figure 7, MSW ash was rich in CaO, Cl, Na_2O, and K_2O, while the content of SiO_2, TiO_2, Al_2O_3, and Fe_2O_3 was relatively low. The content of alkali metal and alkaline earth metal oxides (CaO, Na_2O, and K_2O) in MSW ash reached 72.5%. The alkaline components can be easily evaporated, condensed, and reacted with silicate melts to form low-melting eutectic crystals. This in turn contributes to the formation of melted slag, which may stimulate ash slagging and scaling problems in the flue.[29] The chlorine content in the ash accounted for about 18.5%. Chlorine mainly existed in the form of inorganic chlorine in MSW, and the main form of chlorine in ash was chloride. Chloride was the transmission medium of potassium
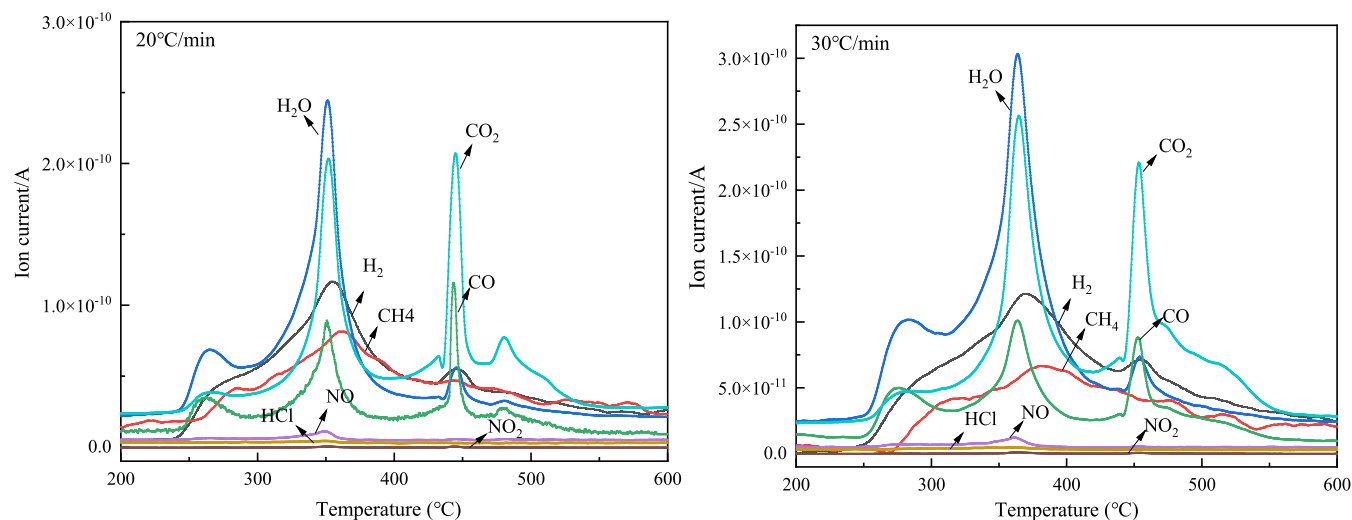
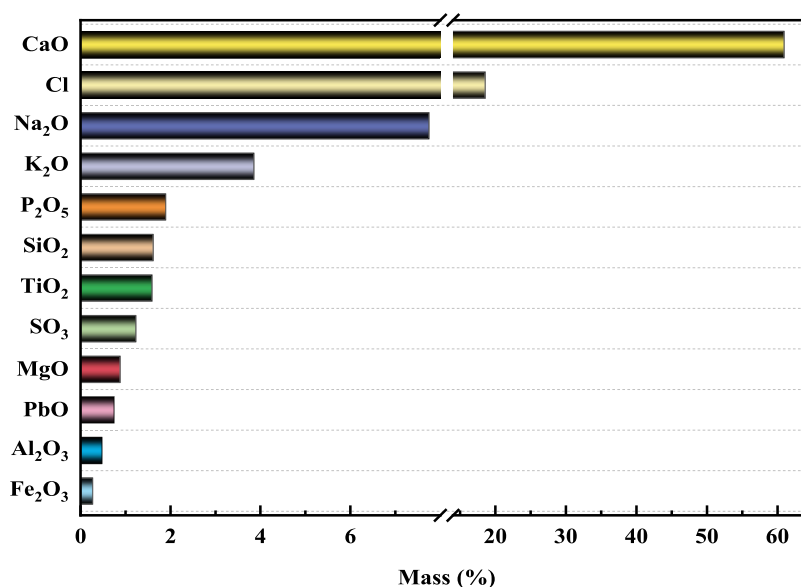**Figure 6.** MS diagram of 30% sorted MSW at different heating rates.

Figure 7. XRF analysis of ash products from 30% sorted MSW.

Table 7. Empirical Indexes Related to Slagging Based on XRF Data[a]

empirical index	formula[32]	30% sorted	deposition criteria
base(B)/acid(A) ratio	$R_{B/A} = (Fe_2O_3 + CaO + MgO + Na_2O + K_2O)/(SiO_2 + Al_2O_3 + TiO_2)$	19.99	$<0.5 \rightarrow$ low $0.5-1.0 \rightarrow$ medium $>1.0 \rightarrow$ high
base/acid ratio (contain P_2O_5)	$R_{B/A+P} = (Fe_2O_3 + CaO + MgO + Na_2O + K_2O + P_2O_5)/(SiO_2 + Al_2O_3 + TiO_2)$	20.50	$<0.5 \rightarrow$ low $0.5-1.0 \rightarrow$ medium $>1.0 \rightarrow$ high
fouling index	$F_u = R_{B/A} \cdot (Na_2O + K_2O)$	1.72	$<0.6 \rightarrow$ low $0.5-40 \rightarrow$ high $>40 \rightarrow$ extremely high
total alkali index	$TA = Na_2O + K_2O$	11.61	$<0.3 \rightarrow$ low $0.3-0.4 \rightarrow$ medium $>0.4 \rightarrow$ high
slagging index	$R_S = R_{B/A} \cdot S$	9.85	$<0.6 \rightarrow$ low $0.6-2.0 \rightarrow$ medium $2.0-2.6 \rightarrow$ high $>2.6 \rightarrow$ extremely high
slagging viscosity index	$S_R = 100 \cdot SiO_2/(SiO_2 + Fe_2O_3 + CaO + MgO)$	2.54	$>78 \rightarrow$ low $66.1-78 \rightarrow$ medium $<66.1 \rightarrow$ high
sintering index	$I = (CaO + MgO)/(Na_2O + K_2O)$	5.33	>2 no sinter
fusion temp index	$F = (SiO_2 + K_2O + P_2O_5)/(CaO + MgO)$	0.12	the higher tendency with higher F value

[a]S: sulfur content (%) based on ultimate analysis; F: fusion temperature index.

and sodium, which would accelerate the high-temperature corrosion of metal surfaces.[30]

The ratio of basic oxides to acidic oxides (B/A) is often used to represent the slagging issue.[31] It can be seen from Table 7 that the B/A ratio of MSW ash was 20.5 due to higher CaO and Na$_2$O. The slagging index reached 9.85, and the risk of slagging of ash was extremely high. The sintering index showed that there was no tendency for the ash of MSW to sinter.

4. CONCLUSIONS

In this paper, the combustion characteristics, kinetic mechanism, and product characteristics of MSW in different sorting scenarios were studied by TG−DSC−FTIR−MS. C,

CCI, D_i, and D_b were the largest when the household waste was sorted by 30%. According to the kinetic analysis, the combustion process of MSW at different heating rates can be regarded as a superposition of a first-order reaction, and the activation energy also showed an increasing trend with the increase in the heating rate. The gaseous product was mainly H$_2$O and CO$_2$, and CH$_4$ and H$_2$ released may be due to a large amount of volatile devolatilization during the second stage. The content of alkali and alkaline earth metal oxides in the ash reached 72.5%, which contributed to the high fouling index with a high risk of slagging.

■ AUTHOR INFORMATION

Corresponding Author

Tianhua Yang — *Key Laboratory of Clean Energy of Liaoning, College of Energy and Environment, Shenyang Aerospace University, Shenyang 110136, China*; Email: thyang@sau.edu.cn

Authors

Bingshuo Li — *Key Laboratory of Clean Energy of Liaoning, College of Energy and Environment, Shenyang Aerospace University, Shenyang 110136, China*; ⊙ orcid.org/0000-0003-4031-2087

Wenkuo Zhang — *Key Laboratory of Clean Energy of Liaoning, College of Energy and Environment, Shenyang Aerospace University, Shenyang 110136, China*

Fan Jia — *Key Laboratory of Clean Energy of Liaoning, College of Energy and Environment, Shenyang Aerospace University, Shenyang 110136, China*

Suping Bai — *Key Laboratory of Clean Energy of Liaoning, College of Energy and Environment, Shenyang Aerospace University, Shenyang 110136, China*

Quan Zhou — *Key Laboratory of Clean Energy of Liaoning, College of Energy and Environment, Shenyang Aerospace University, Shenyang 110136, China*

Complete contact information is available at:
https://pubs.acs.org/10.1021/acsomega.3c07444

Author Contributions

The manuscript was written through contributions of all authors. All authors have given approval to the final version of the manuscript.

Notes

The authors declare no competing financial interest.

■ REFERENCES

(1) Materazzi, M.; Holt, A. Experimental analysis and preliminary assessment of an integrated thermochemical process for production of low-molecular weight biofuels from municipal solid waste (MSW). *Renewable Energy* **2019**, *143*, 663−678.

(2) Tang, L. C.; Chen, M.; Zhang, W.Evaluation of household garbage classification policy based on hardware input-output benefit analysis in Shanghai *China Environ. Sci.* 2022; Vol. *42*, pp 4939−4945.

(3) Huang, H.; Liu, J.; Liu, H.; et al. Dynamic insights into combustion drivers and responses of water hyacinth: evolved gas and ash analyses. *J. Cleaner Prod.* **2020**, *276*, No. 124156.

(4) Lai, Z.; Ma, X.; Tang, Y.; Lin, H. A study on municipal solid waste (MSW) combustion in N_2/O_2 and CO_2/O_2 atmosphere from the perspective of TGA. *Energy* **2011**, *36*, 819−824.

(5) Wienchol, P.; Korus, A.; Szlęk, A.; Ditaranto, M. Thermogravimetric and kinetic study of thermal degradation of various types of municipal solid waste (MSW) under N_2, CO_2 and oxy-fuel conditions. *Energy* **2022**, *248*, No. 123573.

(6) Liu, X.; Asim, T.; Zhu, G.; Mishra, R. Theoretical and experimental investigations on the combustion characteristics of three components mixed municipal solid waste. *Fuel* **2020**, *267*, No. 117183.

(7) Zhang, X.; Li, Y.; Zhang, X.; et al. Co-combustion of municipal solid waste and hydrochars under non-isothermal conditions: thermal behaviors, gaseous emissions and kinetic analyses by TGA-FTIR. *Energy* **2023**, *265*, No. 126373.

(8) Yang, L.; Pang, Q. H.; He, Z.; et al. Nonisothermal thermogravimetric kinetic investigations on combustion behaviors of concomitant biomass from urban plants. *Energy Fuels* **2019**, *33*, 12527−12537.

(9) Zhou, H.; Long, Y. Q.; Meng, A. H.; et al. Classification of municipal solid waste components for thermal conversion in waste-to-energy research. *Fuel* **2015**, *145*, 151−157.

(10) Boumanchar, I.; Chhiti, Y.; Alaoui, F. E. M.; et al. Investigation of (Co)-combustion kinetics of biomass, coal and municipal solid wastes. *Waste Manage.* **2019**, *97*, 10−18.

(11) Rico, J. J.; Pérez-Orozco, R.; Vilas, D. P.; Porteiro, J. TG/DSC and kinetic parametrization of the combustion of agricultural and forestry residues. *Biomass Bioenergy* **2022**, *162*, No. 106485, DOI: 10.1016/j.biombioe.2022.106485.

(12) Cheng, S.; Zhang, H.; Chang, F.; et al. Combustion behavior and thermochemical treatment scheme analysis of oil sludges and oil sludge semicokes. *Energy* **2019**, *167*, 575−587.

(13) Ding, Y.; Liu, J.; Qiu, W.; et al. Kinetics and behavior analysis of lobster shell pyrolysis by TG-FTIR and Py-GC/MS. *J. Anal. Appl. Pyrol.* **2022**, *165*, No. 105580.

(14) Ni, Z.; Bi, H.; Jiang, C.; et al. Influence of biomass on coal slime combustion characteristics based on TG-FTIR, principal component analysis, and artificial neural network. *Sci. Total Environ.* **2022**, *843*, No. 156983.

(15) Zhang, X.; Zhu, S.; Zhu, J.; et al. TG-MS study on co-combustion characteristics and coupling mechanism of coal gasification fly ash and coal gangue by ECSA. *Fuel* **2022**, *314*, No. 123086.

(16) Han, J.; Yao, X.; Zhan, Y.; et al. A method for estimating the higher heating value of biomass-plastic fuel. *J. Energy Inst.* **2017**, *90*, 331−335.

(17) Akahira, T. J.; Sunose, T. Method of determining activation deterioration constant of electrical insulating materials. *Res. Rep. Chiba. Inst. Technol.* **1971**, *16*, 22−31.

(18) Kissinger, H. E. Reaction kinetics in differential thermal analysis. *Anal. Chem.* **1957**, *29*, 1417−1421.

(19) Mishra, A.; Kumari, U.; Turlapati, V. Y.; et al. Extensive thermogravimetric and thermos-kinetic study of waste motor oil based on iso-conversional methods. *Energy Convers. Manage.* **2020**, *221*, No. 113194, DOI: 10.1016/j.enconman.2020.113194.

(20) Hu, J.; Yan, Y.; Evrendilek, F.; et al. Combustion behaviors of three bamboo residues: gas emission, kinetic, reaction mechanism, and optimization patterns. *J. Cleaner Prod.* **2019**, *235*, 549−561.

(21) Wu, X.; Liu, J.; Wei, Z.; et al. Oxy-fuel co-combustion dynamics of phytoremediation biomass and textile dyeing sludge: Gas-to-ash pollution abatement. *Sci. Total Environ.* **2022**, *825*, No. 153656.

(22) Li, W.; Yuan, Z.; Chen, X.; et al. Green refuse derived fuel preparation and combustion performance from the solid residues to build the zero-waste city. *Energy* **2021**, *225*, No. 120252.

(23) Chen, D.; Zhou, J.; Zhang, Q. Effects of heating rate on slow pyrolysis behavior, kinetic parameters and products properties of moso bamboo. *Bioresour. Technol.* **2014**, *169*, 313−319.

(24) Xie, Z.; Ma, X. The thermal behaviour of the co-combustion between paper sludge and rice straw. *Bioresour. Technol.* **2013**, *146*, 611−618.

(25) Kan, T.; Grierson, S.; De Nys, R.; Strezov, V. Comparative assessment of the thermochemical conversion of freshwater and marine micro-and macroalgae. *Energy Fuels* **2014**, *28*, 104−114, DOI: 10.1021/ef401568s.

(26) Wang, Y.; Jia, L.; Guo, J.; et al. Thermogravimetric analysis of co-combustion between municipal sewage sludge and coal slime: combustion characteristics, interaction and kinetics. *Thermochim. Acta* **2021**, *706*, No. 179056.

(27) Gu, X.; Ma, X.; Li, L.; et al. Pyrolysis of poplar wood sawdust by TG-FTIR and Py-GC/MS. *J. Anal. Appl. Pyrolysis* **2013**, *102*, 16−23, DOI: 10.1016/j.jaap.2013.04.009.

(28) Zhang, Y.; Kang, L.; Li, H.; et al. Characterization of moxa floss combustion by TG/DSC, TG-FTIR and IR. *Bioresour. Technol.* **2019**, *288*, No. 121516, DOI: 10.1016/j.biortech.2019.121516.

(29) Yao, X.; Zheng, Y.; Zhou, H.; et al. Effects of biomass blending, ashing temperature and potassium addition on ash sintering behaviour during co-firing of pine sawdust with a Chinese anthracite. *Renewable Energy* **2020**, *147*, 2309−2320.

(30) Niu, Y.; Tan, H.; Hui, S. Ash-related issues during biomass combustion: alkali-induced slagging, silicate melt-induced slagging (ash fusion), agglomeration, corrosion, ash utilization, and related countermeasures. *Prog. Energy Combust. Sci.* **2016**, *52*, 1−61, DOI: 10.1016/j.pecs.2015.09.003.

(31) He, Y.; Chen, X.; Tang, X.; et al. Co-combustion dynamics and products of textile dyeing sludge with waste rubber versus polyurethane tires of shared bikes. *J. Environ. Chem. Eng.* **2023**, *11*, No. 109196.

(32) Chen, C.; Huang, Y.; Qin, S.; et al. Slagging tendency estimation of aquatic microalgae and comparison with terrestrial biomass and waste. *Energy* **2020**, *194*, No. 116889, DOI: 10.1016/j.energy.2019.116889.